Inorg. Chem. **2008**, *47*, 11237−11244

Synthesis, Structure, and Bonding of the Zintl Phase $Ba_3Cd_2Sb_4$

Bayrammurad Saparov, Sheng-qing Xia, and Svilen Bobev*

Department of Chemistry and Biochemistry, University of Delaware, Newark, Delaware 19716

Received August 11, 2008

Reported are the synthesis of the new ternary compound $Ba_3Cd_2Sb_4$ and its structure determination by single-crystal X-ray diffraction. $Ba_3Cd_2Sb_4$ crystallizes with the monoclinic space group *C*2/*m* (No. 12); unit cell parameters $a = 17.835(2)$ Å, $b = 4.8675(5)$ Å, $c = 7.6837(7)$ Å, and $\beta = 112.214(1)°$; $Z = 4$. Its structure can be viewed as made of Ba^{2+} cations and $[Cd_2Sb_4]$ double chains that are interconnected through Sb−Sb bonds to form 2D $^2_\infty[Cd_2Sb_4]^{6-}$ layers. The bonding arrangement in $Ba_3Cd_2Sb_4$ can also be derived from other known structure types that feature similar fragments, such as TiNiSi, Ca_3AlAs_3, and $Ca_5Al_2Sb_6$. Tight-binding linear muffin-tin-orbital band structure calculations are presented as well and show that the constituent elements have closed-shell configurations, indicative of $Ba_3Cd_2Sb_4$ being a Zintl phase with poor metallic behavior. Crystal orbital Hamilton population analyses on selected atomic interactions in this structure are discussed within the context of the site preference, manifested in the mixed-cation compounds and $Ba_{3-x}A_xCd_2Sb_4$, where A = Ca, Sr, Eu, and Yb.

Introduction

The compounds of the least electronegative metals from groups 1 and 2 with the more electronegative metals and metalloids, commonly known as Zintl phases,[1,2] have attracted much interest over the years.[1−19] In particular, very recently, detailed studies on such ternary antimonides with complex structures, such as $Yb_{14}MnSb_{11}$[6a] and $Ca_xYb_{1-x}Zn_2Sb_2$,[6b] have shown that Zintl phases exhibit high thermoelectric figures of merit (*ZT*) and, therefore, can be used as materials for direct thermal-to-electric energy conversion.[6c] Because the thermoelectric properties are closely related to the crystal structures, the search for new pnictides with complicated structures has gained renewed interest. A testament for that is the numerous new compounds reported in the past few years alone: $EuMn_2P_2$,[7] Sr_2MnSb_2,[8] $CaMn_2Sb_2$,[9] $Eu_{10}Mn_6Sb_{13}$,[10] and $Sr_{11}Cd_6Sb_{12}$,[11] among others.

The research in our group has been inspired by these recent discoveries, which motivated us to conduct systematic studies of the fundamental trends in electronic and crystal structures of alkaline-earth and rare-earth metals antimonides and

* To whom correspondence should be addressed. E-mail: bobev@udel.edu. Phone: (302) 831-8720. Fax: (302) 831-6335.

(1) (a) Kauzlarich, S. M., Ed. *Chemistry, Structure, and Bonding of Zintl Phases and Ions*; VCH: New York, 1996; and references cited therein. (b) Corbett, J. D. *Angew. Chem., Int. Ed.* **2000**, *39*, 670–690.
(2) Nesper, R. *Prog. Solid State Chem.* **1990**, *20*, 1–45.
(3) (a) Mao, J.-G.; Xu, Z.-H.; Guloy, A. M. *Inorg. Chem.* **2001**, *40*, 4472–4477. (b) Mao, J.-G.; Goodey, J.; Guloy, A. M. *Inorg. Chem.* **2002**, *41*, 931–937. (c) Gascoin, F.; Sevov, S. C. *Inorg. Chem.* **2002**, *41*, 5920–5924. (d) Gascoin, F.; Sevov, S. C. *Inorg. Chem.* **2003**, *42*, 904–907.
(4) (a) Mills, A. M.; Mar, A. *J. Am. Chem. Soc.* **2001**, *123*, 1151–1158. (b) Mills, A. M.; Mar, A. *Inorg. Chem.* **2000**, *39*, 4599–4607. (c) Mills, A. M.; Deakin, L.; Mar, A. *Chem. Mater.* **2001**, *13*, 1778–1788.
(5) (a) Mudring, A. V.; Corbett, J. D. *Inorg. Chem.* **2005**, *44*, 5636–5640. (b) Ganguli, A. K.; Gupta, S.; Corbett, J. D. *Inorg. Chem.* **2006**, *45*, 196–200.
(6) (a) Brown, S. R.; Kauzlarich, S. M.; Gascoin, F.; Snyder, G. J. *Chem. Mater.* **2006**, *18*, 1873–1877. (b) Gascoin, F.; Ottensmann, S.; Stark, D.; Haile, S. M.; Snyder, G. J. *Adv. Funct. Mater.* **2005**, *15*, 1860–1864. (c) Kauzlarich, S. M.; Brown, S. R.; Snyder, G. J. *Dalton Trans.* **2007**, *21*, 2099–2107.
(7) Payne, A. C.; Sprauve, A. E.; Olmstead, M. M.; Kauzlarich, S. M.; Chan, J. Y.; Reisner, B. A.; Lynn, J. W. *J. Solid State Chem.* **2002**, *163*, 498–505.
(8) Park, S. M.; Kim, S. J.; Kanatzidis, M. G. *Inorg. Chem.* **2005**, *44*, 4979–4982.
(9) Bobev, S.; Merz, J.; Lima, A.; Fritsch, V.; Thompson, J. D.; Sarrao, J. L.; Gillessen, M.; Dronskowski, R. *Inorg. Chem.* **2006**, *45*, 4047–4054.
(10) Holm, A. P.; Park, S. M.; Condron, C. L.; Olmstead, M. M.; Kim, H.; Klavins, P.; Grandjean, F.; Hermann, R. P.; Long, G. J.; Kanatzidis, M. G.; Kauzlarich, S. M.; Kim, S. J. *Inorg. Chem.* **2003**, *42*, 4660–4667.
(11) Park, S. M.; Kim, S. J. *J. Solid State Chem.* **2004**, *177*, 3418–3422.
(12) Xia, S.-Q.; Bobev, S. *J. Am. Chem. Soc.* **2007**, *129*, 4049–4057.
(13) Xia, S.-Q.; Bobev, S. *Chem. Asian J.* **2007**, *2*, 619–624.
(14) Xia, S.-Q.; Bobev, S. *Inorg. Chem.* **2006**, *45*, 7126–7132.
(15) Xia, S.-Q.; Myers, C.; Bobev, S. *Eur. J. Inorg. Chem.* **2008**, 4262–4269.
(16) Saparov, B.; Bobev, S.; Ozbay, A.; Nowak, E. R. *J. Solid State Chem.* **2008**, *181*, 2690–2696.
(17) Bechtel, E.; Cordier, G.; Schäfer, H. *Z. Naturforsch.* **1979**, *B34*, 921–925.
(18) Bechtel, E.; Cordier, G.; Schäfer, H. *J. Less-Common Metals* **1981**, *79*, 131–138.
(19) Xia, S.-Q.; Bobev, S. *J. Comput. Chem.* **2008**, *29*, 2125–2133.

10.1021/ic801530d CCC: $40.75
Published on Web 10/30/2008

bismutides. A number of new Zintl phases have already been synthesized and structurally characterized, including Yb_2CdSb_2 and Ca_2CdSb_2,[12] $Eu_{10}Cd_6Bi_{12}$,[13] $Ba_{11}Cd_8Bi_{14}$,[14] $Mg(Mg_{1-x}Mn_x)_2Sb_2$,[15] and $Eu_{11}Cd_6Sb_{12}$ and $Eu_{11}Zn_6Sb_{12}$.[16] As a part of these ongoing systematic investigations in the A−M−Pn systems, where A = divalent alkaline-earth or rare-earth metals, M = Mn, Zn, and Cd, Pn = pnicogen, we embarked on studying the Ba−Cd−Sb phase diagram. For a long time, only two compounds, $BaCd_2Sb_2$[17] and $BaCdSb_2$,[18] were known, but we recently discovered the new complex Zintl phase $Ba_{11}Cd_6Sb_{12}$.[19] Herein, we describe the continuation of our studies and report on the synthesis, structural characterization, and electronic band structure calculations of the new Zintl phase $Ba_3Cd_2Sb_4$. It crystallizes with a complex monoclinic C-centered structure, which is composed of Cd-centered Sb tetrahedra that share edges. Attempts to synthesize analogues of the title compound resulted in four mixed-cation $Ba_{3-x}A_xCd_2Sb_4$ phases, where A = Ca, Sr, Eu, and Yb. The structure of $Ba_3Cd_2Sb_4$ and its relationship to other well-known structure types, along with cation site preferences in $Ba_{3-x}A_xCd_2Sb_4$, are discussed as well.

Experimental Section

Synthesis. All manipulations were performed inside an argon-filled glovebox with controlled oxygen and moisture levels (below 1 ppm) or under vacuum. The starting materials, pure elements from Alfa or Aldrich with stated purity greater than 99.9%, were used as received. Because the synthesis of $Ba_3Cd_2Sb_4$ employs routine solid-state techniques, only a brief description of the general experimental procedures will be given below. Further details on the synthesis of the Ca-, Sr-, Eu-, and Yb-substituted derivatives of $Ba_3Cd_2Sb_4$, along with specific details on the techniques, are given in the Supporting Information.

Air/moisture-sensitive crystals of the new ternary compound $Ba_3Cd_2Sb_4$ were first obtained from the reaction of Ba, Cd, and Sb metals in a Pb flux. The original reaction was carried out in an attempt to optimize the synthesis of $Ba_{11}Cd_6Sb_{12}$.[19] For that purpose, the elements were weighed in a ratio of Ba:Cd:Sb:Pb = 2:1:2:10. The reactants were loaded in an alumina crucible, which was subsequently enclosed in a fused silica ampule and flame-sealed under vacuum. The evacuated ampule was heated in a muffle furnace to 960 °C at a rate of 200 °C/h, homogenized at 960 °C for 20 h, and then cooled to 500 °C at a rate of 5 °C/h. At this temperature, the excess of molten Pb was removed and two types of small crystals were isolated: needles as a major product and irregular blocks in a lesser amount. Powder and single-crystal X-ray diffraction work proved the needles to be of $Ba_{11}Cd_6Sb_{12}$[19] and the irregular pieces of $Ba_3Cd_2Sb_4$, respectively.

After the structure of $Ba_3Cd_2Sb_4$ was established, the flux synthesis was repeated with the elements loaded in a ratio of Ba:Cd:Sb = 3:2:4, but such a nominal composition, surprisingly, did not produce a pure phase material. From several trial-and-error reactions, it was determined that increasing/decreasing the amount of Pb flux, switching to Cd or Sn flux, and/or including an additional annealing step at 500 °C could not help to eliminate the unwanted side product(s). The best route to make $Ba_3Cd_2Sb_4$ was found when Cd and Sb were used in the exact stoichiometric ratio and Ba was loaded with a slight excess, e.g., Ba:Cd:Sb = 3.5:2:4 (Pb flux), following the above-mentioned heating profile. Analogous reactions were also undertaken in the systems A−M−Pn, where A = Ca, Sr, Eu, and Yb, M = Zn and Cd, and Pn = Sb and Bi, but did not yield any compounds isostructural with $Ba_3Cd_2Sb_4$. Only the reactions with mixed A−Ba cations were successful, which produced the solid solutions $Ba_{3-x}A_xCd_2Sb_4$ (see the Supporting Information). These results are discussed in a broader context later on.

In subsequent experiments aimed at improving the synthesis of $Ba_3Cd_2Sb_4$ and obtaining it in a large yield *without* the use of metal flux, the elements were loaded with the desired stoichiometric ratios and sealed in Nb tubes. Although this experimental procedure proved successful, the polycrystalline products contained multiple phases, and some of them could not be unambiguously identified. Details of the syntheses in Nb tubes are described in the Supporting Information.

Powder X-ray Diffraction. Powder X-ray diffraction patterns were taken at room temperature on a Rigaku MiniFlex powder diffractometer using filtered Cu Kα radiation. The diffractometer was enclosed and operated inside a nitrogen-filled glovebox to allow data collections for air-sensitive materials. Typical runs included $\theta-\theta$ scans ($2\theta_{max} = 80°$) with scan steps of 0.05° and a 10 s/step counting time. Because the samples were mixtures of compounds with complex structures and because of the limited instrument capabilities, the collected powder diffraction patterns were only used for phase identification, which was carried out using the *JADE 6.5* software package. The data analysis of patterns collected before and after exposure of the samples to air showed significant changes, indicative of them being easily oxidized in air.

Single-Crystal X-ray Diffraction and Structure Refinements. Intensity data collections were carried out for a crystal of $Ba_3Cd_2Sb_4$ and four of its substitution derivatives $Ba_{3-x}A_xCd_2Sb_4$ (A = Ca, Sr, Eu, and Yb). Single crystals in all cases were chosen in the glovebox and cut to suitable dimensions for data collection (ca. 0.05−0.07 mm). The crystals were mounted on glass fibers using Paratone-N oil. Data were collected at 120 K on a Bruker SMART CCD-based diffractometer using monochromated Mo Kα radiation. Data acquisition, data integration, and cell refinement were done using the *SMART* and *SAINT+* programs,[20] respectively. Unit cell constants were refined in *SAINT+* using all data. Semiempirical absorption correction based on equivalents was applied using *SADABS*.[21] The structure was solved by direct methods and refined by full-matrix least squares on the F^2 method using *SHELX*.[22] Every step of the structure determination proceeded in a straightforward manner: from the location of all atomic positions by the direct methods solution to the final refinement steps with standardized by STRUCTURE TIDY coordinates.[23] Relevant crystallographic data and structure refinement parameters are given in Table 1. The final positional and equivalent isotropic displacement parameters for $Ba_3Cd_2Sb_4$ are listed in Table 2; Table 3 summarizes some important interatomic distances and angles, respectively. Analogous information for the remaining compounds with mixed cations is summarized in Tables S1−S8 (Supporting Information), along with a graphical representation of the structure with anisotropic displacement parameters. Further details on all structure refinements, in the form of CIF files, can also be found in the Supporting Information. The CIFs have also been deposited with Fachinformationszentrum Karlsruhe, 76344 Eggenstein-Leopoldshafen, Ger-

(20) (a) *SMART NT*, version 5.63; Bruker Analytical X-ray Systems, Inc.: Madison, WI, 2003. (b) *SAINT*, version 6.45; Bruker Analytical X-ray Systems, Inc.: Madison, WI, 2003.
(21) *SADABS NT*, version 2.10; Bruker Analytical X-ray Systems, Inc.: Madison, WI, 2001.
(22) *SHELXTL*, version 6.12; Bruker Analytical X-ray Systems, Inc.: Madison, WI, 2001.
(23) Gelato, L. M.; Parthe, E. *J. Appl. Crystallogr.* **1987**, *20*, 139–143.

Table 1. Selected Crystallographic Data and Structure Refinement Parameters for $Ba_3Cd_2Sb_4$ and Its Substitution Derivatives $Ba_{3-x}A_xCd_2Sb_4$ (A = Ca, Sr, Eu, and Yb)

empirical formula	$Ba_3Cd_2Sb_4$	$Ba_{2.93(1)}Ca_{0.07}Cd_2Sb_4$	$Ba_{2.37(1)}Sr_{0.63}Cd_2Sb_4$	$Ba_{2.58(1)}Eu_{0.42}Cd_2Sb_4$	$Ba_{2.94(1)}Yb_{0.06}Cd_2Sb_4$
fw, g/mol	1123.82	1119.44	1092.25	1129.96	1126.14
data collection temp, K	120(2)	120(2)	120(2)	120(2)	120(2)
radiation, wavelength, Å	Mo Kα, λ = 0.710 73	Mo Kα, λ = 0.710 73	Mo Kα, λ = 0.710 73	Mo Kα, λ = 0.710 73	Mo Kα, λ = 0.710 73
crystal system	monoclinic	monoclinic	monoclinic	monoclinic	monoclinic
space group, *Z*	*C2/m* (No. 12), 2	*C2/m* (No. 12), 2	*C2/m* (No. 12), 2	*C2/m* (No. 12), 2	*C2/m* (No. 12), 2
unit cell dimens[a]	*a* = 17.835(2) Å	*a* = 17.796(9) Å	*a* = 17.596(1) Å	*a* = 17.649(2) Å	*a* = 17.790(5) Å
	b = 4.8675(5) Å	*b* = 4.876(3) Å	*b* = 4.8825(4) Å	*b* = 4.8793(5) Å	*b* = 4.875(2) Å
	c = 7.6837(7) Å	*c* = 7.654(4) Å	*c* = 7.5310(6) Å	*c* = 7.5676(7) Å	*c* = 7.656(2) Å
	β = 112.214(1)°	β = 112.129(5)°	β = 111.640(1)°	β = 111.680(1)°	β = 112.108(4)°
unit cell volume, $Å^3$	617.53(10)	615.2(6)	601.39(8)	605.59(10)	615.1(3)
density (ρ_{calc}), g/cm^3	6.044	6.044	6.032	6.197	6.080
abs coeff (μ), mm^{-1}	21.307	21.266	22.629	22.525	21.675
final *R* indices [a] [$I > 2\sigma(I)$]	R1 = 0.0164	R1 = 0.0259	R1 = 0.0162	R1 = 0.0146	R1 = 0.0198
	wR2 = 0.0393	wR2 = 0.0558	wR2 = 0.0368	wR2 = 0.0348	wR2 = 0.0460

[a] $R1 = \sum||F_o| - |F_c||/\sum|F_o|$, $wR2 = [\sum[w(F_o^2 - F_c^2)^2]/\sum[w(F_o^2)^2]]^{1/2}$, and $w = 1/[\sigma^2F_o^2 + (AP)^2 + BP]$, $P = (F_o^2 + 2F_c^2)/3$. A and B are weight coefficients.

Table 2. Atomic Coordinates and Equivalent Isotropic Displacement Parameters (U_{eq}[a]) for $Ba_3Cd_2Sb_4$[b]

atom	Wyckoff position	*x*	*y*	*z*	U_{eq}, $Å^2$
Ba1	4*i*	0.14194(2)	0	0.59031(5)	0.0105(1)
Ba2	2*a*	0	0	0	0.0094(1)
Cd	4*i*	0.33167(3)	0	0.02826(6)	0.0107(1)
Sb1	4*i*	0.20771(2)	0	0.19654(6)	0.0095(1)
Sb2	4*i*	0.49775(2)	0	0.31514(5)	0.0099(1)

[a] U_{eq} is defined as one-third of the trace of the orthogonalized U_{ij} tensor. [b] The atomic coordinates for $Ba_{3-x}A_xCd_2Sb_4$ (A = Ca, Sr, Eu, and Yb) given in the Supporting Information.

Table 3. Selected Bond Distances (Å) and Angles (deg) in $Ba_3Cd_2Sb_4$[a]

within the $^2_\infty[Cd_2Sb_4]^{6-}$ layers		between Ba^{2+} and the $^2_\infty[Cd_2Sb_4]^{6-}$ layers	
Sb1−Cd (×2)	2.9125(4)	Ba1−Sb1 (×2)	3.5319(4)
Sb1−Cd	2.9531(6)	Ba1−Sb1 (×2)	3.5911(4)
Sb2−Sb2	2.8114(8)	Ba1−Sb1	3.6351(6)
Sb2−Cd	2.9488(6)	Ba1−Cd (×2)	3.7002(5)
Cd−Sb1 (×2)	2.9125(4)	Ba1−Sb2 (×2)	3.7453(5)
Cd−Sb2	2.9488(6)	Ba2−Sb1 (×2)	3.4314(5)
Cd−Sb1	2.9531(6)	Ba2−Sb2 (×2)	3.4441(4)

[a] Tetrahedral angles: Sb1−Cd−Sb1 101.95(1)°; Sb2−Cd−Sb1 112.29(2)°; Sb1−Cd−Sb2 113.09(1)°; Sb1−Cd−Sb1 113.36(2)°.

many: depository numbers CSD-419719 ($Ba_3Cd_2Sb_4$); CSD-419720 ($Ba_{2.93(1)}Ca_{0.07}Cd_2Sb_4$); CSD-419721 ($Ba_{2.37(1)}Sr_{0.63}Cd_2Sb_4$); CSD-419722 ($Ba_{2.58(1)}Eu_{0.42}Cd_2Sb_4$); CSD-419723 ($Ba_{2.94(1)}Yb_{0.06}Cd_2Sb_4$).

Electronic Structure Calculations. Tight-binding linear muffin-tin orbital (TB-LMTO)[24] electronic structure calculations were carried out using the *LMTO-4.7* package.[25] The method uses the atomic sphere approximation; exchange and correlation were treated in the local density approximation.[26] All relativistic effects except for spin−orbital coupling were taken into account by using the scalar relativistic approximation.[27] Space was filled automatically with overlapping Wigner−Seitz (WS) atomic spheres. No empty spheres were used in current calculations. To compare the energy difference between selected models, the WS radii were kept as follows: Ba = 2.33 Å, Sr = 2.21 Å, Cd = 1.61 Å,and Sb = 1.69 Å. The basis sets consisted of 5*d*, 6*s*, and 6*p* orbitals for Ba, 4*d*, 5*s*, and 5*p* orbitals for Sr and Cd, and 5*s*, 5*p*, and 5*d* orbitals for Sb. The Ba 5*d*, Sr 4*d*, and Sb 5*d* orbitals were treated by the downfolding technique.[28] The crystal orbital Hamilton population (COHP) method[29] was employed for analysis of the chemical bonding. In the provided COHP plot, the curves were inverted so that the positive regions indicate bonding and negative regions show antibonding interactions, and the Fermi level was selected as a reference point (0 eV). The self-consistent charge-density iterations were performed using 216 irreducible *k* points in the Brillouin zone, and the *k*-space integrations were performed by the tetrahedron method.[30]

In order to calculate two different models for the ordering of the cations in $Ba_2SrCd_2Sb_4$, the symmetry of $Ba_3Cd_2Sb_4$ was reduced from the original space group *C2/m* to *Cm*. This allowed the cations within and between the layers to be treated separately.

Results and Discussion

Structure and Bonding. $Ba_3Cd_2Sb_4$ (Figure 1) crystallizes in what appears to be a new monoclinic structure type with a Pearson's code *mC*18. The structure is centrosymmetric with the space group *C2/m* (No. 12), and it contains five crystallographically unique sites in the asymmetric unit, all in special positions: two Ba sites, one Cd site, and two Sb sites (Table 2). Inspection of Pearson's handbook[31] and the Inorganic Crystal Structure Database (ICSD)[32] reveals that there are several other monoclinic structure types with identical Wyckoff sequences that show similar, yet subtly different, bonding patterns. The similarities and the differences between them are discussed later.

The structure of $Ba_3Cd_2Sb_4$ is best described as a polyanionic $^2_\infty[Cd_2Sb_4]^{6-}$ sublattice made up of $CdSb_4$ tetrahedra and Ba^{2+} cations enclosed between them, as shown in Figure 1. The $CdSb_4$ tetrahedra share corners to form $^1_\infty[CdSb_3]$ chains, running along the crystallographic *b* direction. Following the nomenclature proposed by Liebau,[33] these should be classified as *Einereinfach* chains, a motif that is

(24) (a) Andersen, O. K. *Phys. Rev. B* **1975**, *12*, 3060–3083. (b) Andersen, O. K.; Jepsen, O. *Phys. Rev. Lett.* **1984**, *53*, 2571–2574. (c) Andersen, O. K.; Jepsen, O.; Glötzel, D. *Highlights of Condensed Matter Theory*; Bassani, F., Fumi, F., Tosi, M. P., Eds.; North Holland: New York, 1985. (d) Andersen, O. K. *Phys. Rev. B* **1986**, *34*, 2439–2449.

(25) Jepsen, O.; Andersen, O. K. *TB-LMTO-ASA Program*, version 4.7; Max-Planck-Institut für Festkörperforschung: Stuttgart, Germany, 1998.

(26) Von Barth, U.; Hedin, L. *J. Phys. C* **1972**, *5*, 1629–1642.

(27) Koelling, D. D.; Harmon, B. N. *J. Phys. C* **1977**, *10*, 3107–3114.

(28) Lambrecht, W. R. L.; Andersen, O. K. *Phys. Rev. B* **1986**, *34*, 2439–2449.

(29) Dronskowski, R.; Blöchl, P. *J. Phys. Chem.* **1993**, *97*, 8617–8624.

(30) Blöchl, P. E.; Jepsen, O.; Andersen, O. K. *Phys. Rev. B* **1994**, *49*, 16223–16233.

(31) Villars, P., Calvert L. D., Eds. *Pearson's Handbook of Crystallographic Data for Intermetallic Phases*, 2nd ed.; American Society for Metals: Materials Park, OH, 1991; and the desktop edition, 1997.

(32) ICSD Database, Fachinformationszentrum, Karlsruhe, Germany, 2008.

(33) Liebau, F. *Naturwissenschaften* **1962**, *49*, 481–491.

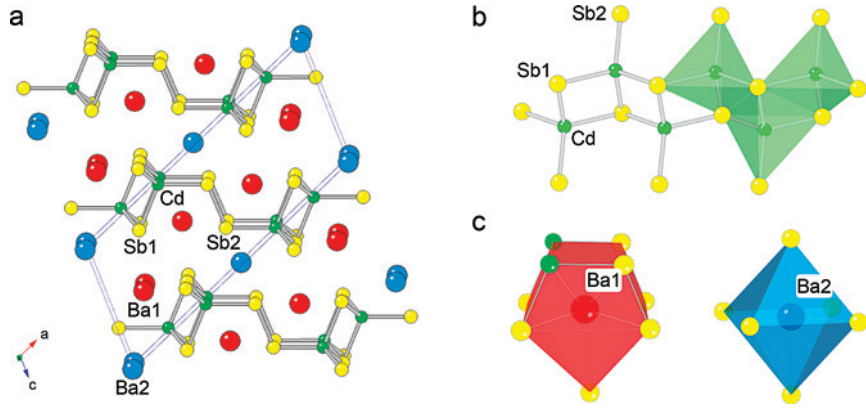

Figure 1. (a) Perspective view of the monoclinic structure of $Ba_3Cd_2Sb_4$, viewed down the *b* axis. The Sb atoms are shown as yellow spheres; the Cd atoms are drawn as light-green spheres. The two types of Ba atoms, the inter- and intralayer ones, are colored differently, in light-blue and in red, respectively. The unit cell is outlined. (b) $^1_\infty[Cd_2Sb_4]^{8-}$ double chains of edge-shared tetrahedra, shown in a different orientation. (c) Close view of the coordination polyhedra of Ba1 and Ba2. Relevant distances are provided in Table 3.

very common among the orthosilicates and germanates.[34] Similar structural fragments are found in many Zintl phases as well, for example, $^1_\infty[AlAs_3]^{6-}$ in Ca_3AlAs_3[34] and $^1_\infty[SnP_3]^{5-}$ in $Sr_5Sn_2P_6$,[35] to name a few.[36] In $Ba_3Cd_2Sb_4$, the $^1_\infty[CdSb_3]$ chains are "dimerized" through shared vertices and edges, resulting in $[Cd_2Sb_4]$ double chains (Figure 1b). The latter are further connected to their neighbors via an *exo*-Sb−Sb bond to form 2D layers, $^2_\infty[Cd_2Sb_4]^{6-}$. They propagate parallel to the $(20\bar{1})$ plane and are well separated by the large Ba^{2+} cations (shortest interlayer distance greater than 4.7 Å). The Cd−Sb distances fall in the narrow range from 2.9125(4) to 2.9531(5) Å, and the Sb−Cd−Sb angles vary between 101.95(1)° and 113.36(2)° (Table 3). These metric parameters are comparable to the ones reported for other intermetallic compounds with structures based on $CdSb_4$ tetrahedra, such as $Sr_{11}Cd_6Sb_{12}$,[11] Yb_2CdSb_2 and Ca_2CdSb_2,[12] $Sr_9Cd_{4.49(1)}Sb_9$,[37] $Ba_{21}Cd_4Sb_{18}$,[38] etc. Almost all interatomic distances in the substitution derivatives $Ba_{3-x}A_xCd_2Sb_4$ (A = Ca, Sr, Eu, and Yb) are systematically shorter than those in $Ba_3Cd_2Sb_4$, following the contraction of the unit cell volume (Table 1). Notable exceptions are the Sb−Sb bonds, which seem to elongate upon mixing of the larger Ba^{2+} cations with the smaller Ca^{2+}, Sr^{2+}, Eu^{2+}, and Yb^{2+} cations, which are discussed next.

The Sb−Sb distance in $Ba_3Cd_2Sb_4$ is 2.8114(8) Å, appreciably shorter than the 2.908 Å contacts in elemental Sb.[39] This is not unusual given that d_{Sb-Sb} on the order of 2.8 Å are well-known for compounds with related exo-bonded structural elements, such as $Sr_{11}Cd_6Sb_{12}$,[11] $Eu_{11}Cd_6Sb_{12}$,[16] $Ba_{11}Cd_6Sb_{12}$,[19] and $Eu_5In_2Sb_6$,[40] as well as some simpler binaries, KSb[41] and Rb_5Sb_4,[42] among others. Other intermetallics, whose structures feature isolated Sb_2 dimers, for example, $Ba_{21}Cd_4Sb_{18}$,[38] Cs_4Sb_2,[43] $Eu_{11}InSb_9$,[44] $Yb_{11}GaSb_9$,[45] and $Ca_{21}Mn_4Sb_{18}$,[46] are reported to have slightly longer d_{Sb-Sb} distances, ranging from 2.84 to 2.90 Å. The linear Sb_3^{7-} fragments in $A_{14}MnSb_{11}$ (A = Ca, Sr, and Ba)[47] exhibit even larger Sb−Sb separation, on the order of 3.2−3.3 Å. Noteworthy, as mentioned above, is the fact that the Sb−Sb distances are elongated upon shortening of the unit cell axes; for example, in $Ba_{2.37(1)}Sr_{0.63}Cd_2Sb_4$, where the volume change is most significant, ca. −2.5% (Table 1), the Sb−Sb bonds are 2.8291(8) Å, almost 0.8% longer compared to the Sb−Sb bonds in $Ba_3Cd_2Sb_4$. A similar subtlety of the bonding was previously discussed for the pair of isostructural compounds $Sr_{11}Cd_6Sb_{12}$ and $Ba_{11}Cd_6Sb_{12}$,[11,19] where regardless of the large volume change d_{Sb-Sb} remains virtually unchanged. All of the above are indicative of a very strong covalency of the Sb−Sb interactions. More in-depth analysis of the chemical bonding in such isolated or linked Sb_2 dimers can be found elsewhere.[19]

There are two types of Ba atoms: intralayer Ba atoms, which reside within the $[Cd_2Sb_4]$ layers (labeled Ba1), and interlayer Ba atoms, which are positioned between adjacent layers (labeled Ba2). As seen from Figure 1c, the coordination environments of the two cations are very different: Ba1 is surrounded by seven Sb atoms with average d_{Ba-Sb} = 3.624 Å, while Ba2 is at the center of a nearly regular octahedron of six Sb atoms (average d_{Ba-Sb} = 3.440 Å). Similar differences in the cation coordination have been noted for Ca_2CdSb_2 and Yb_2CdSb_2[12] and are attributed to having an

(34) Cordier, G.; Schäfer, H. *Angew. Chem., Int. Ed. Engl.* **1981**, *20*, 466.
(35) Eisenmann, B.; Jordan, H.; Schäfer, H. *J. Less-Common Metals* **1986**, *116*, 251–258.
(36) Isosteric polyanionic chains are reported in many other intermetallics including Sr_3InP_3, Eu_3InP_3, Ca_3AlSb_3, Ca_3AlAs_3, Ca_3InP_3, and Ca_3GaAs_3, but in the literature, many of these compounds are erroneously assigned their own structure types.[31] Careful inspection of the structures suggests that they are all with the orthorhombic Ca_3AlAs_3 type structure.
(37) Xia, S.-Q.; Bobev, S. *J. Am. Chem. Soc.* **2007**, *129*, 10011–10018.
(38) Xia, S.-Q.; Bobev, S. *Inorg. Chem.* **2008**, *47*, 1919–1921.
(39) Pauling, L. *The Nature of the Chemical Bond*, 3rd ed.; Cornell University Press: Ithaca, NY, 1960.
(40) Park, S. M.; Choi, E. S.; Kang, W.; Kim, S. J. *J. Mater. Chem.* **2002**, *12*, 1839–1843.
(41) Hönle, W.; Vonschnering, H. G. *Z. Kristallogr.* **1981**, *155*, 307–314.
(42) Gascoin, F.; Sevov, S. C. *Inorg. Chem.* **2001**, *40*, 5177–5181.
(43) Hirschle, C.; Röhr, C. *Z. Anorg. Allg. Chem.* **2000**, *626*, 1992–1998.
(44) Xia, S.-Q.; Hullmann, J.; Bobev, S.; Ozbay, A.; Nowak, E. R.; Fritsch, V. *J. Solid State Chem.* **2007**, *180*, 2088–2094.
(45) Bobev, S.; Fritsch, V.; Thompson, J. D.; Sarrao, J. L.; Eck, B.; Dronskowski, R.; Kauzlarich, S. M. *J. Solid State Chem.* **2005**, *178*, 1071–1079.
(46) Holm, A. P.; Olmstead, M. M.; Kauzlarich, S. M. *Inorg. Chem.* **2003**, *42*, 1973–1981.
(47) Rehr, A.; Kuromoto, T. Y.; Kauzlarich, S. M.; Delcastillo, J.; Webb, D. *J. Chem. Mater.* **1994**, *6*, 93–99.

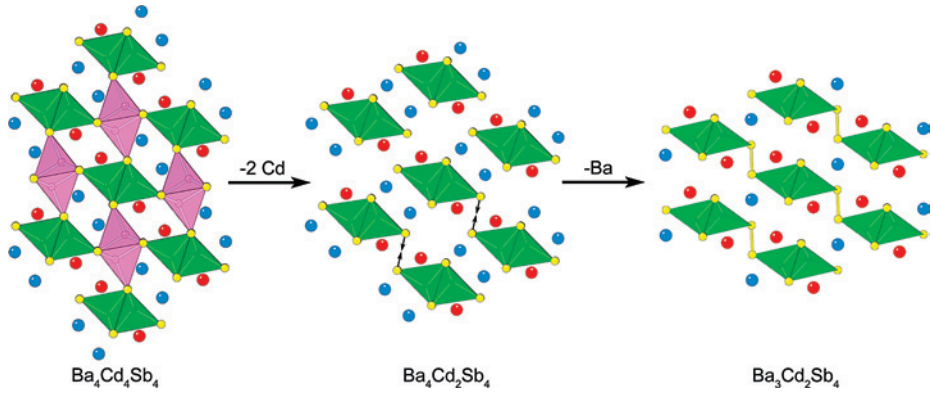

Figure 2. Schematic representation of how the $Ba_3Cd_2Sb_4$ structure can be derived from the hypothetical compound $Ba_4Cd_4Sb_4$ (TiNiSi structure type). Emphasized is the creation of $^2_\infty[Cd_2Sb_4]^{6-}$ layers by removal of half of the Cd atoms in the 3D $[Cd_4Sb_4]$ network. See the text for further discussion.

effect on the different packings of the $^2_\infty[CdSb_2]^{4-}$ layers in the two structures. We attempted to extend this chemistry into the $Ba_3Cd_2Sb_4$ structure and explore the phase space for its analogues with other divalent cations. So far, we only have succeeded in the synthesis of $Ba_{3-x}A_xCd_2Sb_4$ (A = Ca, Sr, Eu, and Yb). Although these are solid solutions, on basis of single-crystal X-ray diffraction work, we find that only the Ba2 site is prone to substitution by another divalent metal; the Ba1 site "exhibits" stricter Ba preference. These considerations are the subject of a more comprehensive discussion in the following section.

Structural Relationships and Electron Count. A different description of the $Ba_3Cd_2Sb_4$ structure can be proposed once its close relationship with the ubiquitous TiNiSi[31] structure type is recognized. This structure boasts a polyanionic 3D framework of corner- and edge-shared tetrahedra and cations residing within its channels. Using an imaginary cutting and pasting, as schematically illustrated in Figure 2, the structure of $Ba_3Cd_2Sb_4$ can be conveniently derived from that of the hypothetical BaCdSb compound (TiNiSi type), reformulated for convenience as $Ba_4Cd_4Sb_4$. It requires removal of a selected half of the $CdSb_4$ tetrahedra from the framework,[48] in a way that isolated $^1_\infty[Cd_2Sb_4]^{8-}$ chains of edge-shared tetrahedra are left behind. Next, through a small distortion, these fragments are brought closer together and joined via adjacent Sb apexes to form $^2_\infty[Cd_2Sb_4]^{6-}$ layers, with exactly the same topology as the layers in $Ba_3Cd_2Sb_4$. Finally, because of the formation of *exo*-Sb−Sb bonds and the changed crystal packing requirements, one of the Ba^{2+} cations becomes redundant and needs to be removed. The outlined imaginary transformation accounts for not only the structure but also the composition of the title compound according to the balanced equation

$$Ba_3Cd_2Sb_4 = Ba_4Cd_4Sb_4 - 2Cd - Ba$$

One obvious "parent" structure is that of $Ca_5Al_2Sb_6$,[49] featuring $^1_\infty[Al_2Sb_6]^{10-}$ double chains, made up of chains of corner-shared tetrahedra, $^1_\infty[AlSb_3]^{6-}$, joined together via adjacent Sb apexes. As discussed above, a similar building block is central to the $Ba_3Cd_2Sb_4$ structure as well. Following this line of thought, the $^2_\infty[Cd_2Sb_4]^{6-}$ layers in $Ba_3Cd_2Sb_4$ can then be viewed as polymerized analogues of the hypothetical $^1_\infty[Cd_2Sb_6]^{12-}$ double chains with the $Ca_5Al_2Sb_6$ type structure.[49] This condensation occurs through two sets of opposing Sb corners, a total of four Sb atoms per formula unit.

Two more interesting similarities between the $Ba_3Cd_2Sb_4$ structure and $RE_4Ni_2InGe_4$ (RE = Dy, Ho, Er, and Tm),[50] on the one hand, and $Sr_3Al_2Ge_4$,[51] on the other hand, deserve special mention too. The former (Pearson's code *mC*22) can be viewed as a "stuffed" variant of $Ba_3Cd_2Sb_4$ (Pearson's code *mC*18) because both have layers, $[Cd_2Sb_4]$ and $[Ni_2Ge_4]$, with identical topology. The difference between the two structures is in the interlayer space, where in the case of $Ba_3Cd_2Sb_4$ only Ba atoms are present, whereas in $RE_4Ni_2InGe_4$ one additional RE and In atoms are "inserted" within the $RE_3Ni_2Ge_4$ substructure. The structure of the other compound, $Sr_3Al_2Ge_4$,[51] as the stoichiometry suggests, is even closer to that of $Ba_3Cd_2Sb_4$ but not the same. The monoclinic $Sr_3Al_2Ge_4$ (Pearson's code *mC*18) features $^1_\infty[Al_2Ge_4]$ double chains, which are the same as their $^1_\infty[Cd_2Sb_4]$ counterparts in $Ba_3Cd_2Sb_4$. The difference here is in the way the chains are linked together: in the $Sr_3Al_2Ge_4$ structure, the condensation is through Ge zigzag chains, not exo bonds as in $Ba_3Cd_2Sb_4$.[52] In essence, this makes the bridging atoms not two- but rather three-bonded, which will have implications on the formal electron count (below). We note here that such a type of connectivity between tetrahedral building blocks is less common for the Pn-rich compounds and is reported for complex structures such as $Ba_{11}Cd_8Bi_{14}$,[14] $BaIn_2Sb_4$,[53] and $Ba_2Sn_3Sb_6$.[54]

Last, following this description of structural relations and prior to a more in-depth analysis of the electronic structure, it is useful to discuss the electron count using the Zintl rules.[1,2] Following them, $Ba_3Cd_2Sb_4$ should be a charge-balanced Zintl phase according to the formulation $(Ba^{2+})_3[(4b-$

(48) Notice here that if Cd atoms are removed differently, one would obtain basic arrangements in either the Ca_2CdSb_2 or Yb_2CdSb_2 structures.[12]
(49) Cordier, G.; Czech, E.; Jakowski, M.; Schäfer, H. *Rev. Chim. Miner.* **1981**, *18*, 9–18.
(50) Salvador, J. R.; Kanatzidis, M. G. *Inorg. Chem.* **2006**, *45*, 7091–7099.
(51) Wendorff, M.; Röhr, C. *Z. Naturforsch.* **2007**, *B62*, 1071–1082.
(52) For clarity, graphical representations and side-by-side comparisons among these structures are provided as Supporting Information.
(53) Kim, S.-J.; Hu, S.; Uher, C.; Kanatzidis, M. G. *Chem. Mater.* **1999**, *11*, 3154–3159.
(54) Lam, R.; Mar, A. *Inorg. Chem.* **1996**, *35*, 6959–6963.

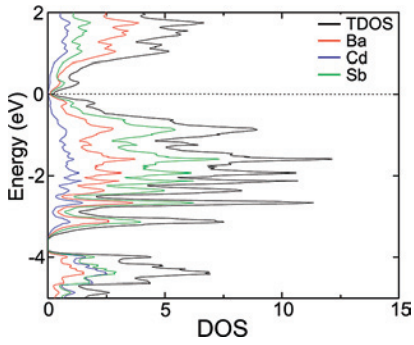

Figure 3. Projected total and partial DOS for $Ba_3Cd_2Sb_4$. Contributions from different atoms are color-coded.

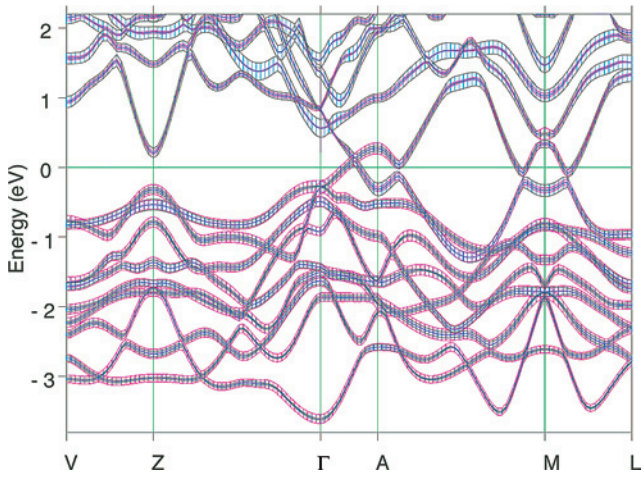

Figure 4. Band diagram for $Ba_3Cd_2Sb_4$, showing the fat-band representations for the Ba 5*d* orbitals (green) and the Sb 5*p* orbitals (magenta).

$Cd^{2-})_2(3b\text{-}Sb^0)_2(2b\text{-}Sb^{1-})_2]$. Similarly, the Zintl reasoning provides the following electron count for $Sr_3Al_2Ge_4$ − $(Sr^{2+})_3[(4b\text{-}Al^{1-})_2(3b\text{-}Ge^{1-})_4]$. The fact that both structures have closed-shell configurations for the constituent elements might explain the subtle structural change discussed herein; $Sr_3Al_2Ge_4$ with the same structure as $Ba_3Cd_2Sb_4$ would have been electron-deficient because each two-bonded Ge will require two extra electrons to complete its octet, thus dictating the need for zigzag chains. Using the same simplistic point of view, one might also argue that $Ba_5Cd_2Sb_6$ with the $Ca_5Al_2Sb_6$ structure should also be electron-deficient, which might be the driving force for interconnecting the $[Cd_2Sb_6]^{12-}$ fragments via sharing of four Sb atoms, as seen in the $Ba_3Cd_2Sb_4$ structure.

Electronic Structure. Selected results from the density functional theory calculations on $Ba_3Cd_2Sb_4$ are presented in Figures 3 and 4. According to the computed band structure, the bonding in this compound is almost fully optimized, confirming the formal electron count after the Zintl concept.[1,2] There are only a few bands cutting through the Fermi level at different *k* points, and they originate mainly from Ba and Sb states. As is evident from the total and partial density of states (DOS) plots (Figure 3) and the fat-band representations (Figure 4), the states just below and above the Fermi level have significant Sb 5p and Ba 5d contributions, respectively, indicative of considerable cation−anion orbital mixing. This suggests that the Ba−Sb interactions

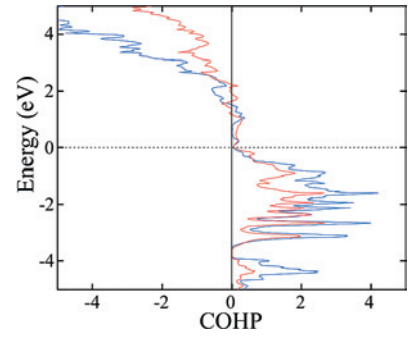

Figure 5. COHP curves for Ba1−Sb and Ba2−Sb interactions. The blue line represents interactions of the intralayer Ba cation (Ba1 in 4*i*) with the next-nearest Sb anions; the red one represents interlayer Ba (Ba2 in 2*a*). Their coordination polyhedra are shown in Figure 1c.

are not completely ionic and that the Ba cations are not just "spectators", as implied by the classic Zintl reasoning.[1,2] As a consequence and as it is clearly represented in the total DOS plot (Figure 3), the gap (also known as a pseudogap) at the Fermi level nearly disappears. Therefore, although a charge balance is formally achieved (see above), $Ba_3Cd_2Sb_4$ is not expected to be a semiconductor like some other Zintl phases.[1,2] Such a result is in agreement with earlier reports that show that semimetallic or poorly metallic behavior is not uncommon even for simpler structures, for example, Ca_5Ge_3[55] and Na_3AuIn_2,[56] among others.

Cation Site Preferences. As was already discussed, despite the large number of reactions conducted in different systems under different conditions, only $Ba_3Cd_2Sb_4$ and four mixed compounds $Ba_{3-x}A_xCd_2Sb_4$ (A = Ca, Sr, Eu, and Yb) could be obtained. The solubility ranges for the smaller Ca^{2+} and Yb^{2+} are quite narrow, while the larger Sr^{2+} and Eu^{2+} can substitute Ba^{2+} to a greater extent, indicating the importance of the cation size. In all cases, only the interlayer Ba atoms (Ba2) can be partially replaced.

To study in more detail the nature of the Ba1−Sb and Ba2−Sb interactions in order to better understand the tendency of the two cation sites to be "colored" differently (terminology adopted after Miller's interpretations of the "coloring problem" in intermetallics[57]), we calculated the COHPs for all of the alkaline-earth metal−pnicogen interactions (Figure 5). The average integrated COHP values reveal that Ba2−Sb interactions are significantly stronger, according to their average integrated COHP values (−iCOHP), being 0.988 eV. For comparison, −iCOHP for Ba1−Sb is 0.803 eV, which could be related to the pronounced differences in the Ba1−Sb and Ba2−Sb distances (Table 3). The d-orbital population for the intralayer Ba1 atoms is lower than that for interlayer Ba2 atoms, 1.344 and 1.385, respectively. Following again Miller's ideas[57] and using the atomic orbital populations (AOPs) to predict possible site preferences, one could readily suggest that in $Ba_{3-x}A_xCd_2Sb_4$ (A = Ca, Sr, Eu,

(55) Mudring, A.-V.; Corbett, J. D. *J. Am. Chem. Soc.* **2004**, *126*, 5277–5281.
(56) Li, B.; Corbett, J. D. *Inorg. Chem.* **2005**, *44*, 6515–6517.
(57) (a) Miller, G. J. *Eur. J. Inorg. Chem.* **1998**, *5*, 523–536. (b) Han, M.-K.; Miller, G. J. *Inorg. Chem.* **2008**, *47*, 515–528. (c) Richter, K. W. *J. Alloys Compd.* **2002**, *338*, 43–50.

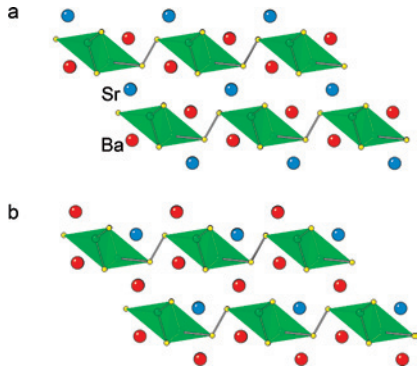

Figure 6. Polyhedral views of the two hypothetical models for $Ba_2SrCd_2Sb_4$, used for calculations (a) with Sr atoms placed in the interlayer position and (b) with Sr atoms placed in one of the intralayer positions. The Sr and Ba atoms are shown in blue and red, respectively.

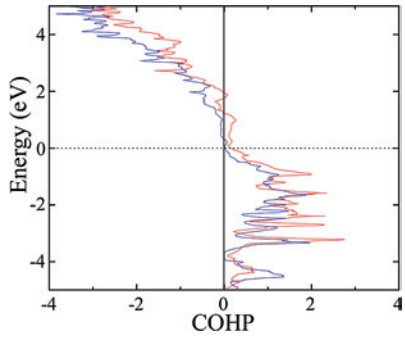

Figure 7. COHP curves for Sr−Sb interactions in $Ba_2SrCd_2Sb_4$. The blue line represents the intralayer interactions, and the red line represents the interlayer interactions.

and Yb), the less electronegative element, Ba (Pauling electronegativity of 0.9[39]), will prefer the site with lower AOP, i.e., the intralayer 4*i* Wyckoff position. On the contrary, the more electronegative Ca, Sr, Eu, and Yb (Pauling electronegativities around or greater than 1.0[39]) will be more likely to occupy the site with higher electron density, which is the interlayer 2*a* site in the current case.

In order to further investigate and to compare and contrast the two cation positions, calculations were performed for two hypothetical models for $Ba_2SrCd_2Sb_4$ (Figure 6): (1) with Sr placed in the interlayer position, while Ba resides within the $^2_\infty[Cd_2Sb_4]^{6-}$ layers, and (2) with Sr placed in one of the intralayer positions (symmetry lowered to *Cm*). Not surprisingly, the calculations indicated the former to be more stable, with the difference in the total energy between the two cases being 0.515 eV/cell. The corresponding Sr−Sb COHP curves are provided in Figure 7, and the integrated COHP values are tabulated in Table S9 (Supporting Information). These results are in excellent agreement with the discussion above on the crystallographic data, confirming that bonds are stronger when Sr are between layers and not the other way around and that Sr atoms in the interlayer position have higher electron density (as judged from the AOP) than Sr atoms located within the layers. Another interesting comparison can be made between the intralayer Ba atoms in $Ba_3Cd_2Sb_4$ and the intralayer Sr atoms in $Ba_2SrCd_2Sb_4$ in terms of their bonding and their orbital populations (Tables S9 and S10 in the Supporting Information). The data indicate that Ba−Sb interactions are stronger than the Sr−Sb ones and that the Ba AOP is higher than the Sr AOP. These computational results confirm that while Sr^{2+} is more likely to exchange Ba^{2+} in the interlayer positions than in the intralayer positions, complete substitution will not be favored.

Therefore, because $Ba_3Cd_2Sb_4$ is expected to be the most stable phase, one can readily explain why the interlayer Ba is never replaced 100%. Such a conclusion is fully supported by the basic geometric principles and chemical logic as well; an interlayer cation is octahedrally coordinated by Sb, with four Cd atoms as the second nearest neighbors ($d_{Ba-Cd} > 4$ Å), while the intralayer cation is surrounded by seven Sb and two Cd (Figure 1c). Thus, it is reasonable to expect that the larger Ba will prefer the site with higher coordination number, while Sr and the remaining smaller cations will prefer the octahedral site. One might also use the simplistic chemical rationale to speculate that the greater mismatch between the ionic radii of Ba^{2+} (1.36 Å) and Ca^{2+} (1.00 Å) compared to Ba^{2+} and Sr^{2+} (1.16 Å),[58] for example, is the reason why Ca substitutes only about 7 atom % Ba at the Ba2 site, while Sr substitutes more than 60 atom %. A similar explanation can be provided for $Ba_{2.58(1)}Eu_{0.42}Cd_2Sb_4$ and $Ba_{2.94(1)}Yb_{0.06}Cd_2Sb_4$, especially after it is recognized that the ionic radii of Eu^{2+} (1.17 Å) and Yb^{2+} (1.02 Å) are almost the same as those of Sr^{2+} and Ca^{2+}, respectively.[58] A related discussion on the cations as structure-directing factors can be found in several earlier publications.[12,37,59]

Conclusions

A new ternary compound $Ba_3Cd_2Sb_4$ has been synthesized and structurally characterized by single-crystal X-ray diffraction. The compound crystallizes in a monoclinic crystal system, in the space group *C*2/*m*, and its structure can be viewed as 2D $[Cd_2Sb_4]$ layers made up of $CdSb_4$ tetrahedra, separated by Ba cations. The tetrahedra are edge-shared and linked through Sb_2 dimers. Concerning the structure, a number of analogies could be drawn with other known structure types, featuring similar building blocks, such as the $Ca_5Al_2Sb_6$ structure,[49] the Ca_2CdSb_2 and Yb_2CdSb_2 structures,[12] and, of course, the TiNiSi structure.[31] Similar bonding arrangements have been reported previously for $RE_4Ni_2InGe_4$ (RE = Dy, Ho, Er, and Tm)[50] and $Sr_3Al_2Ge_4$;[51] however, they are not identical with the structure in question. Although reactions intended to make a series of isostructutural compounds failed, four mixed $Ba_{3-x}A_xCd_2Sb_4$ phases, where A = Ca, Sr, Eu, and Yb, were also synthesized. It was observed that, in all four compounds, only the interlayer Ba atoms can be replaced. TB-LMTO calculations showed that the interlayer Ba site has higher electron density and interactions of interlayer atoms with surrounding Sb atoms show stronger covalent character. The results of the calculations also show that, even though interlayer Ba atoms are more

(58) Shannon, R. D. *Acta Crystallogr.* **1976**, *A32*, 751–767.
(59) Seo, D. K.; Corbett, J. D. *J. Am. Chem. Soc.* **2000**, *122*, 9621–9627.

likely to be replaced, Ba atoms themselves are favored more in that position.

Acknowledgment. S.B. acknowledges financial support from the University of Delaware and the Petroleum Research Fund administrated by the American Chemical Society.

Supporting Information Available: X-ray crystallographic file in CIF format, representations of the crystal structure with anisotropic displacement parameters, tables with the corresponding atomic coordinates and interatomic distances for $Ba_{3-x}A_xCd_2Sb_4$ (A = Ca, Sr, Eu, and Yb), integrated COHP, and side-by-side comparisons among the structures of $Ba_3Cd_2Sb_4$, $Sr_3Al_2Ge_4$, and $Er_4Ni_2InGe_4$. This material is available free of charge via the Internet at http://pubs.acs.org.

IC801530D